Nanoscale

Accepted Manuscript

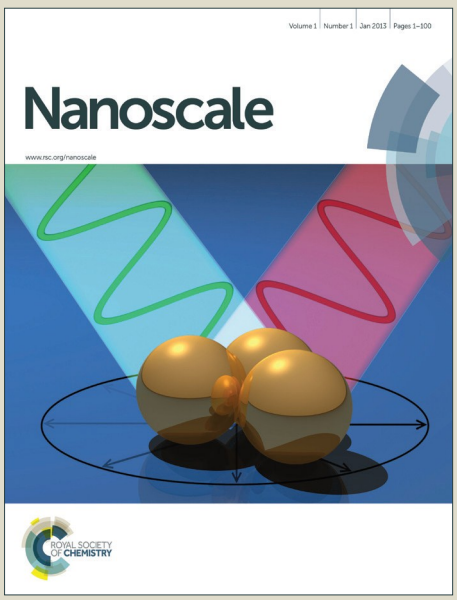

ROYAL SOCIETY OF CHEMISTRY

www.rsc.org/nanoscale

Journal Name

ARTICLE

Electrical release of dopamine and levodopa mediated by amphiphilic β-cyclodextrins immobilized on polycrystalline gold

Received 00th January 20xx,
Accepted 00th January 20xx

DOI: 10.1039/x0xx00000x

www.rsc.org/

Giulia Foschi,[a, ‡] Francesca Leonardi,[b,‡] Angela Scala,[c] Fabio Biscarini,[a] Alessandro Kovtun,[b] Andrea Liscio,[b] Antonino Mazzaglia[*,c] and Stefano Casalini[*,a]

Vesicles of cationic amphiphilic β-cyclodextrins have been immobilized on polycrystalline gold by exploiting the chemical affinity between their amino groups and Au atoms. The presence of cyclodextrins have been widely investigated by means of AFM, XPS, kelvin probe and electrochemical measurements. This multi-functional coating confers distinct electrochemical features such as pH-dependent behavior and partial/total blocking properties towards electro-active species. The host-guest property of β-cyclodextrins has been successfully exploited in order to trap drugs, like dopamine and levodopa. The further release of these drugs was successfully achieved by providing specific electrical stimuli. This proof-of-concept led us to the fabrication of an electronic device (*i.e.* organic transistor) capable to dispense both dopamine and levodopa in aqueous solution.

Introduction

In the last decade, the proper combination of material science and nanotechnology has led to the so-called "nanoarchitectonics"[1]. The proper processing of nano-compounds and eventually their immobilization on a substrate of interest allows one to fabricate new multi-functional interfaces, which can be exploited in different fields such as electrochemical capacitors, super-capacitors, biosensors, drug release systems, bioreactors etc.[2]

Within this context, cyclodextrins (CyDs) can be proficiently exploited. CyDs are trunk-shaped cyclic oligosaccharides composed by 6, 7 or 8 α-D-glucopyranose units, known as α-, β- and γ-CyDs respectively[3]. Among the wide library of CyD-derivatives, amphiphilic CyDs (ACyDs) are promising candidates because they outdo the natural CyDs features[4]. ACyDs are synthesized by grafting an hydrophobic moiety (*viz.* alkylthio chain) and an hydrophilic functionality (*viz.* polyethylene glycol chain, PEG) on the narrow and the wide rim of CyDs[5]. This backbone enables to form bilayer vesicles in aqueous solution, in which the lipophilic chains are hydrophobically entangled yielding the core of the vesicle membrane, whereas the hydrophilic chains are exposed to the outer environment (see Fig.1a). These vesicles show multi-functional properties since they act as "liposomes" entirely composed by macrocyclic hosting molecules. Nowadays, a wide library of ACyDs is available owing to their versatile synthesis, and they can be classified as a function of their outer charges (*viz.* non-ionic, cationic and anionic ones). For instance, the presence of various terminal groups (*i.e.* -NH_2 group) allows ACyDs to adhere and pass through the cell membrane[6,7]. Furthermore, they can host and/or entrap a wide library of guests, such as antiviral[8] and antimitotic drugs[9], metal-photosensitizers for photo-activated or photo-independent anticancer therapies[10–12], or DNA for gene delivery[13]. A proper combination of ACyDs and metals enables to achieve a multi-functional vector for phototherapeutics purposes[14,15]. As a result, cationic AβCyDs endowed with porphyrins can be successfully casted on quartz substrates yielding photo-responsive films[16] or forming bilayer vesicles capable to strongly interact with gold nanoparticles (AuNPs)[15]. The molecular interaction between cationic AβCyD vesicles and AuNPs has been widely investigated, pointing out the crucial role exerted by -NH_2 group[15]. The preferential coordination of AuNPs with the amino group, rather than the thioether group, agrees with a poor accessibility of the sulphur atom because of its steric hindrance imposed by the whole structure of the vesicles. These nanoconstructs can entrap polar and/or apolar drugs, thus forming delivery systems with potentially high therapeutic efficacy.

In parallel, organic electronics has witnessed a dramatic boost towards biomedical applications, since organic transistors, such as the electrolyte-gated organic field-effect transistors (EGOFETs), can be successfully operated in aqueous

[a] Università degli Studi di Modena e Reggio Emilia, Dipartimento di Scienze della Vita, via Campi 183, I-41100 Modena, Italy.
[b] CNR-ISOF Istituto per la Sintesi Organica e la Fotoreattività, v. Gobetti n.101, I-40129 Bologna (Italy).
[c] CNR-ISMN Istituto per lo Studio dei Materiali Nanostrutturati, c/o Dipartimento di Scienze Chimiche dell'Università di Messina, V. le F. Stagno d'Alcontres 31, I-98166, Messina, Italy.
Dr. F. Leonardi and Dr. S. Casalini are actually working at the Institut de Ciéncia de Materials de Barcelona (ICMAB-CSIC), 08193 Bellaterra (Spain).
†† Authors who equally contributed.
* Corresponding author.
Electronic Supplementary Information (ESI) available: Kelvin probe, AFM and electrochemical data are reported. Furthermore, the chemical backbone of both types of cyclodextrins are shown. See DOI: 10.1039/x0xx00000x

environment without any additional capping layer[17]. This enabled to fabricate low-power electronic devices whose operational voltages are lower than 1V[18]. Their extreme versatility along with easy materials processing led to the fabrication of wearable electronics not only on skin[19], but also on internal organs (*viz.* heart, brain, spinal cord etc.)[20–23]. For instance, a multi-tasking platform was recently designed and applied onto skin, whose layout brings together mechanical sensors, non-volatile memory and a complex system of drug release[24]. Another stretchable platform was successfully implanted onto the spinal cord in order to provide both electrical recording/stimuli and a local drug delivery[25].

Here, our main objective was the immobilization of cationic A*ϐ*CyD vesicles onto Au electrodes. Although a wide literature is present on the exploitation of cyclodextrins as electrode modifiers[26], it has been solely studied the role of the surface tension of a solid support upon the A*ϐ*CyD-based vesicles adsorption. In case of poor chemical affinity between vesicles and substrate, the adsorption of these vesicles can yield monolayer and/or bilayer coatings[27]. In our approach, we take advantage of the chemical affinity between Au and amine groups in order to develop a multi-functional electrode by means of an one-step process. This multi-functional electrode is capable to release electrically neurotransmitters, such as dopamine (DA) and levodopa (L-DOPA). Furthermore, we have integrated our A*ϐ*CyD-coated electrode in an EGOFET layout, aiming at the development of smart technology for biomedical applications.

Results and discussion

Kelvin Probe and X-Ray Photoemission

The simple immersion of Au electrode in a solution containing cationic AβCyD vesicles (see Fig.1a) allowed us to yield a stable coating on this metal (see experimental section).

Kelvin Probe (KP) and X-Ray Photoemission Spectroscopy (XPS) measurements have been performed. KP has allowed us to monitor the contact potential difference (CPD) of electrode at each functionalization step (see Fig.S1 in ESI)[28]. Although this technique provides a qualitative view of the Au surface due to the complexity of the AβCyD coating, clear changes are induced. A more accurate description has been achieved by means of XPS. In fact, the vesicles immobilization induces the presence of nitrogen atom on the Au surface. For this reason, N 1s spectra has been monitored, showing unambiguously the presence of AβCyD after the Au immersion in the vesicles solution. In particular the presence of two nitrogen chemical species have been detected such as ammonium (NH_3^+) and amino (NH_2) groups, set respectively at 402.3 eV and 400.2 eV, in good agreement with literature[15,28] (see Fig.1b). Quantitatively, we observe a changing of the relative intensities of the two peaks where the NH_2/NH_3^+ ratio, which passes from 1.3(±0.2) to 2.8(±0.3). The doubling of this value strongly indicates the presence of dopamine that possesses an additional amino group (*i.e.* NH_2). This proof is also confirmed by the increasing of the signal of nitrogen with respect to the gold one (data not shown).

AFM and Electrochemical assessment of A*ϐ*CyDs functionalization

The adsorption of bilayer vesicles is a complex process, which involves not only the transition from free vesicles in solution to immobilized ones onto a solid support, but also other phenomena such as rupture, coalescence and fusion[29,30]. Although a detailed study of the coating morphology is beyond the scope of this work, we have performed AFM on flat region of Au electrode (see Fig.1c). By using the Height-Height Correlation Function (HHCF), morphological descriptors such as the root mean square roughness (σ_{rms}), the lateral correlation length (ξ) and the roughness exponent (α) have been extracted[31,32], as shown in Fig.1d.

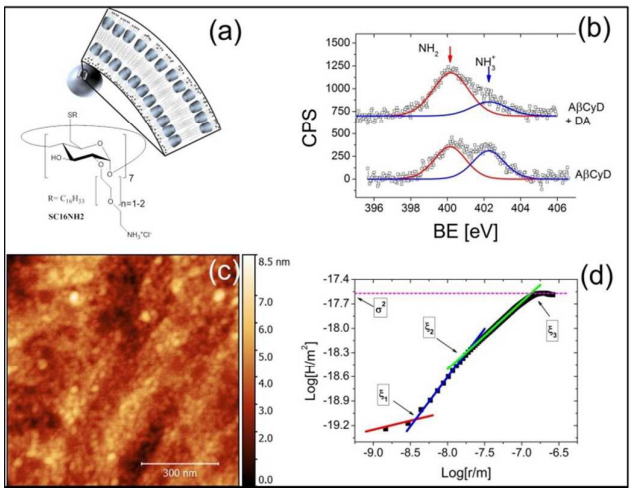

Figure 1 a) Chemical backbone of A*ϐ*CyD and its assembly yielding a cationic vesicle. **b)** Comparison of the N 1s spectra for the samples of (up) AβCyD and (down) AβCyD loaded by DA. **c)** AFM image (1μm²) of Au functionalized by cationic A*ϐ*CyD vesicles. **d)** Log-Log plot of the height-height correlation function. Red, blue, green and pink lines are linear fits.

Moving from bare (see Fig.S2) to A*ϐ*CyD-coated Au (see Fig.1c, d), we observe a rougher surface together with a lower number of correlation lengths. These can be considered two distinct fingerprints of the A*ϐ*CyDs immobilization (see Table S1). In particular, the bare Au features σ_{rms} as low as 0.89(±0.01)nm with respect to A*ϐ*CyDs-coated one, whose σ_{rms} is equal to 1.64(±0.01)nm. Concerning functionalized Au, ξ_1 and ξ_2 are ascribable to the circular species, whose correlation lengths are equal to 3.7(±0.1)nm and 18.6(±0.3)nm respectively. The size discrepancy is relevant with respect to the radius (*i.e.* 30nm) of the free vesicles in solution, thus deeper surface analysis are required in order to elucidate the effective reason of this shrinkage[33]. Finally, ξ_3 of A*ϐ*CyD-coated Au can be safely ascribed to the atomic ordering of Au, because this correlation length is similar to the uncoated one.

These cationic vesicles are adsorbed onto Au surface due to their amino groups that are situated at the end of oligo-ethylene glycol chain in AβCyDs hydrophilic portion[15]. To support our rationale, we have performed the same

experiment by using non-ionic AβCyD vesicles, as reference experiment. These vesicles feature hydroxyl groups instead of amine ones, and they cannot be immobilized onto Au (see Fig.S3). Cyclic voltammetry (CV) and electrochemical impedance spectroscopy (EIS) have been performed as described in the experimental section. The peak to peak distance (ΔE_p), namely the difference of the cathodic and anodic peaks, is a parameter directly connected to the reversibility of the electron transfer (ET) between ferricyanide and Au. ΔE_p higher than 60 mV means a lowering of the electron transfer rate with respect to the ideal redox reaction[34]. In parallel, EIS set to the redox potential of ferricyanide allowed us to extract the charge transfer resistance (R_{CT}) and capacitance (C) by means of the Randles circuit[35]. As shown in Fig.S4 and Fig.S5, this ensemble of parameters describes quantitatively the unsuccessful immobilization of non-ionic vesicles compared with cationic ones.

A further experimental evidence of the immobilization of the cationic vesicles on Au electrode was gained from the electrochemical study of the redox signal of ferricyanide as a function of pH (viz. from 3 to 12). The cationic A*β*CyD vesicles bear amine groups that are protonated/unprotonated by changing pH, hence the overall positive charges onto Au. As a result, CV (see Fig.2a) and EIS (see Fig.2b) measurements were performed as described in the experimental section. As shown in Fig.2c, acidic and neutral environment show values centred around 100mV of ΔE_p featuring a quasi-reversible redox reaction. Beyond neutral condition, ΔE_p has a linear increase featuring a slope of 35(±3) mV/pH because of a slower ET rate than the acidic/neutral state. Furthermore the redox potential of ferricyanide is invariant as a function of pH, in fact its redox reaction does not involve protons. The impedance spectroscopy confirms this trend. Regarding to EIS measurements, the R_{CT} is irrespective of pH variations from 3 to 7, whereas the alkaline range induces a linear increase of the overall impedance with slope equal to 0.71(±0.04) kΩ/pH (see Fig.2d). All these evidences show how $[Fe(CN)_6]^{3-/4-}$ interact electrostatically with the cationic vesicles adsorbed onto Au. In particular, acidic and neutral environments keep protonated the amino groups present of the vesicles maximizing the electrostatic attraction between them and ferricyanide. Moving towards alkaline buffer, the amino group gets uncharged due to its deprotonation (pK_a equal to 9)[36], and this weakens this type of interaction. For this reason the overall ET slowing down at alkaline environment is perfectly coherent to the electrostatic view. Within this context, an additional proof of the A*β*CyD vesicles grafting on Au electrode is the blocking properties towards positively electro-active species. As a result, DA and L-DOPA are electrochemical active featuring well-known faradaic current ranging from +200mV and +300mV (*vs.* Ag/AgCl)[37]. By comparing the bare and vesicles-coated Au, it is clear how the adsorbed A*β*CyD vesicles are blocking the redox reaction of these two compounds with respect to the bare electrode as shown in Fig.3a,b.

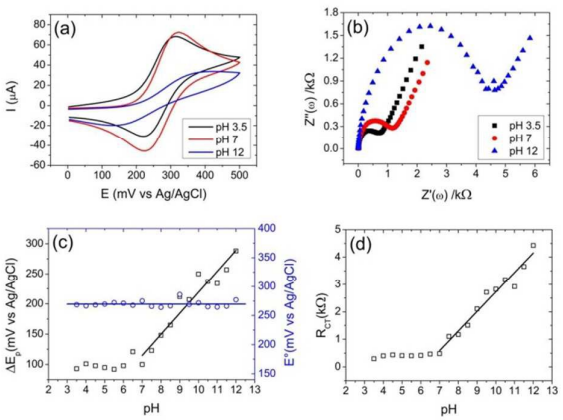

Figure 2 (a) Cyclic voltammograms and (b) Nyquist plots of the redox signal of $[Fe(CN)_6]^{2-/3-}$ at acidic (pH 3.5), neutral (pH 7) and alkaline (pH 11) solutions. (c) Peak-to-peak distance (black empty squares) and redox potential (blue empty circles) are plotted as a function of pH. (d) pH-dependence of the charge transfer resistance

In terms of current response, the faradaic current of the bare Au is turned into a purely capacitive after the surface functionalization. This further proof stems from the above-mentioned electrostatic screening of the vesicles-based coating towards positively charged species such as DA and L-DOPA at neutral pH[38].

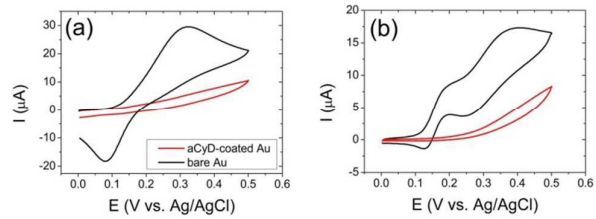

Figure 3 Overlay of cyclic voltammogramms for bare (black line) and A*β*CyDs coated Au (red line) corresponding to 1mM of DOPA (a) and L-DOPA (b) in a phosphate buffered solution (100mM at pH 7).

Electrical release of dopamine and L-DOPA

As mentioned in the introduction, A*β*CyDs vesicles give rise not only to electrostatic interaction tunable by pH, but they can act as drug "*catcher*" by means of host-guest interaction. Since *β*CyDs have been widely used to host dopamine and its derivatives[39–43], we have decided to incubate our functionalized electrodes in DA and L-DOPA solutions (see experimental section). These A*β*CyDs-coated and drug-loaded electrodes have been electrically stressed by iterative voltammetric cycles centred at the redox potential of DA/L-DOPA. As shown in Fig.4, 20 cycles are sufficient to follow the total disappearance of the anodic peak. This means that iterative cycling can induce the detachment of DA and L-DOPA trapped in the cationic vesicles. Since it is known that DA and its derivatives can be partially adsorbed on bare Au[44,45], we compared A*β*CyDs-coated Au (see Fig.4a, Fig.4c and Fig.4e) and the bare one (see Fig.4b, Fig.4d and Fig.4f) after the immersion in DA/L-DOPA solutions. This allowed us to

undertake an accurate evaluation of the AβCyDs role during the electrical release. Firstly, the AβCyDs-coated electrode shows more resolved anodic peak (see Fig.4a and Fig.4c) than the bare one (see Fig.4b and Fig.4d) featuring a more efficient ET. On contrary, the cathodic peak is completely quenched for AβCyDs-coated Au, because the vesicles-based coating screens electrostatically the Au electrode against positive species, as previously described. Furthermore, the kinetics of the release has been characterized by monitoring the anodic peak. The kinetic mechanism has been fitted as a first order reaction (see Fig.4e and see Fig.4f):

$$[A_{ads}] \xrightarrow{potential} [A_{free}]$$

in which $[A_{ads}]$ is the drug trapped, $[A_{free}]$ is the specie released by the electrical field.

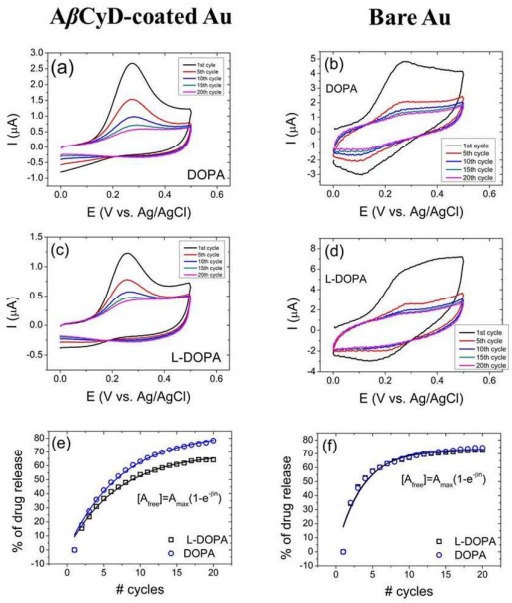

Figure 4 Electrical release of DA and L-DOPA for AβCyDs-coated Au (a, c, e) and bare one (b, d, f). Fit of the electrical release of both drugs corresponding to functionalized (e) and bare Au (f).

The dataset has been successfully fitted by the following equation

$$[A_{free}] = A_{\max}\left(1 - e^{-\beta n}\right)$$

where A_{max} is the maximum amount of DA/L-DOPA released, β is the kinetic rate and n is the number of voltammetric cycles. As you can see in the Table 1,

Table 1 A_{max}, β and $n_{1/2}$ have been extracted by the 1st order reaction equation and listed here

	A_{max} (%)	β (cycle^{-1})	$n_{1/2}$ (cycle)
AβCyD coated Au [DA]	84(±2)	0.14(±0.01)	4.9(±0.3)
AβCyD coated Au [L-DOPA]	69(±2)	0.14(±0.01)	4.9(±0.3)
Bare Au [DA]	74(±2)	0.27(±0.02)	2.6(±0.2)
Bare Au [L-DOPA]	72(±2)	0.29(±0.03)	2.4(±0.2)

the release mediated by AβCyD vesicles has the same half lifetime ($n_{1/2}$), however the overall amount of released DA is higher than L-DOPA. On contrary, the $n_{1/2}$ of bare Au is half compared to the functionalized Au, featuring a faster process, whose A_{max} is the same for both drugs. This agrees with an aspecific adsorption of both neurotransmitters onto the bare Au with respect to the host-guest interaction occurring when Au is functionalized by AβCyD vesicles.

Drug dispenser based on electrolyte-gated organic field-effect transistor (EGOFET)

In light of these properties, it has been decided to integrate AβCyD coated-Au electrode as the gate of an EGOFET. This device can be coupled to aqueous solutions, because they are water-stable and capable to work at low operational voltages (*i.e.* <1V). Furthermore, these devices are extremely sensitive towards surface modifications by exploiting organic compounds and/or bio-species[46–50]. In particular, we have monitored the different states of this gate surface: i) bare, ii) AβCyDs grafting, iii) DA/L-DOPA loading and iv) its release. I-V transfer (see Fig.5a) and output (see Fig.5b) characteristics have been consequently acquired. The electrical performances of the reference EGOFET (*i.e.* uncoated Au electrode) are aligned to the standard behaviour of a water-gate organic transistor, whose working principle is based on the capacitive coupling between the gate electrode (*i.e.* polycrystalline Au) and the organic semiconductor (*i.e.* pentacene). Small hysteresis and leakage current at the nA scale are fingerprints that no electrochemical doping is occurring during the whole experiment[51,52]. It has been extracted field-effect mobility (see Fig.5c) and the plateau current (see Fig.5d) from I-V transfer and output characteristics for each surface treatment. These two parameters are consistent, because the subsequent addition of biochemical species on the gate electrode are responsible of a progressive resistive drop at the gate/electrolyte interface[49,50]. This is also coherent with the CPD trend extracted by the KP measurements, which monitors the effective changes of surface potential due to the presence of different distribution of dipoles onto the metal surface[53,54].

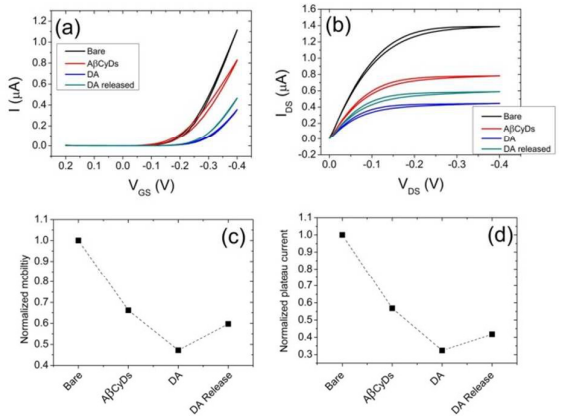

Figure 5 I-V transfer (a) and (b) output characteristics corresponding to each step of the functionalization protocol. (c) Mobility and (d) the maximum current of the output characteristics are plotted for each functionalization step.

Furthermore, it has been successfully verified how the electrochemical release of drug can be directly managed by an EGOFET (see Fig.6a,b) with respect to the previous experiment, where the drug release has been achieved by using an electrochemical cell. After the usual characterization of the different functionalization steps (Fig.6a), source and drain electrodes have been grounded and short-circuited, and it has been monitored the gate-source current (I_{GS}) sweeping from 0V to 1.1V(Fig.6b).

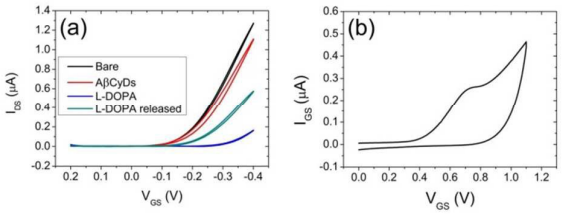

Figure 6 I-V transfer (a) and output (b) characteristics for bare (black line) and A*β*CyDs functionalized (red line) gate electrode. I_{GS} *vs.* V_{GS} plot corresponding to the redox behavior of in-situ release of L-DOPA.

An anodic peak has been observed around 700mV owing to the drug release. This setup exploits the gate electrode as working electrode, whereas the organic semiconductor acts as a counter electrode. By comparing EGOFET and a standard electrochemical cell, the presence of an insulating film of pentacene onto source and drain along with the absence of a reference electrode gives rise to a potential discrepancy in the two systems.

Experimental

Preparation of AβCyDs solution and Au functionalization

Both cationic and non-ionic A*β*CyDs vesicles (see Fig.1a) of SC16NH2/SC16OH were prepared following the protocol published elsewhere[33]. Briefly, SC16NH2/SC16OH were dissolved in dichloromethane (0.1mg/ml) and slowly evaporated under N_2. This organic film was re-dispersed in aqueous solution (bi-distilled water) by using ultrasonic bath for 5h at RT. In parallel, polycrystalline Au wires (∅ 1mm) were cleaned as follows: (i) immersion in a concentrated H_2SO_4 at 100°C for 1h; (ii) 20 cycles of electropolish sweeping the potential from 0V to 1.5V in H_2SO_4 (1M)[55]. These electrodes have been then immersed in aqueous solution containing the cationic vesicles overnight. The final step was a further immersion of the A*β*CyDs-coated Au in an aqueous solution of DA or L-DOPA (1mM) for 30min.

Kelvin Probe

Kelvin Probe measurements were performed under ambient conditions using 2 mm diameter gold tip amplifier (Ambient Kelvin Probe Package from KP Technology Ltd.). The technique provides a voltage resolution of about 5 mV. Calibration and monitoring of the probe was performed using a freshly prepared gold surface. A comprehensive description of the technique can be found in Baikie et al.[56]

X-ray photoemission

The XPS spectra were recorded in UHV condition ($5 \cdot 10^{-10}$ mbar) with an Phoibos 100 hemispherical energy analyser (Specs) using Mg Kα radiation (ħω=1253.6 eV). The X-ray power was 250 W. The spectra were recorded in the constant analyser energy (CAE) mode with analyser pass energies of 20 eV. Peaks were fit with symmetric Voigt function processed by CasaXPS v.2.3.16 software. The calibration of the binding energy was done by using the Au $4f_{7/2}$ peak (BE=84.0eV) from the substrate and the C 1s signal at 285.0eV from surface contamination.

AFM Imaging

AFM Solver Platform SMENA (NT-MDT Moscow, Russia) operated in intermittent contact mode was used for scanning the surface of polycrystalline Au functionalized by cationic A*β*CyDs vesicles (see Fig.1c). In particular, AFM has been performed onto golden slides purchased from Arrandee (Germany) and flame annealed as described in their datasheet. This instrument is equipped with a camera for positioning the cantilever on selected areas of the sample. AFM data analysis was carried out with Gwyddion 2.30 software.

Electrochemical measurements

The electrochemical measurements are performed by an usual three-electrodes cell connected to a potentiostat/galvanostat μ-Autolab type III (Metrohm Italiana S.r.l., Varese, Italy), using a polycrystalline Au wire, as working electrode (WE), functionalized with the above-mentioned protocol; a Pt sheet and Ag/AgCl were used as counter (CE) and reference (RE) electrodes respectively. The ferricyanide signal has been monitored by cyclic voltammetry (CV) and electrochemical impedance spectroscopy (EIS). The former has been carried out between 0V and +500mV (*vs.* Ag/AgCl) with a scan rate of

100mV/s. The latter has been performed fixing the set-point voltage at the redox potential (namely E°) of $[Fe(CN)_6]^{3-/4-}$ with an amplitude of 10mV scanning from 10^5 Hz to 10^1 Hz. The Nyquist plots have been fit by using the Randles equivalent circuit, which allows us to extract the charge transfer resistance (R_{CT}) and the capacitance (C) of the material deposited onto the working electrode. The electrolytic solutions with a known pH consisted of phosphate buffer (100mM) and NaCl (0.1M). The pH adjustments have been obtained by using small aliquots of NaOH and HCl.

Electrical characterization of electrolyte-gated organic field-effect transistor (EGOFET)

Test-patterns have been purchased from Fondazione Bruno Kessler (Trento, Italy). The substrate is quartz (optical grade) with a roughness lower than 2nm. The Au leads are 40nm thick with an adhesive layer of Cr (3-4nm thick). The W/L ratio is around 2000. The pentacene deposition was performed by thermal sublimation in ultrahigh vacuum with a base pressure of 5×10^{-8} mbar at a rate of 7.5 Å min^{-1} on the substrate held at room temperature. The pentacene film was 15 nm thick (~10 monolayers, ML) as previously published[55,57]. Source, drain and gate electrodes were connected to a Keithley 2612 Source Meter. The electrical response was acquired by means of home-built test-pattern holder. This system offers a compact layout and an easy-to-use monitoring of the electrical performances of our EGOFETs. The electrical measurements were carried out in lab atmosphere. The I-V transfer characteristics were performed by sweeping the gate-source voltage (V_{GS}) from +0.5V to -0.5V while leaving the drain-source voltage (V_{DS}) constant at -0.1V (linear regime) for the reference device. The I-V output characteristics were carried out by sweeping V_{DS} from 0V to -0.5V and V_{GS} from 0V to -0.5V with step of 0.1V. The electrical measurements after DA adsorption were carried out by sweeping V_{GS} from +0.2V to -0.4V with V_{DS} =-0.1V. The V_{GS} scan rate is around 20mV/s and 80mV/s for transfer and output characteristics respectively. The electrical release of DA and L-DOPA through an EGOFET has been carried out scanning the V_{GS} from 0V to 1.1V. Source and drain electrodes have been short-circuited and grounded, therefore the device has been operated as a two-electrodes system.

Conclusions

This work was focused on the chemical adsorption of AβCyD vesicles onto Au by exploiting the well-known affinity between amino groups and this metal. The vesicles adsorption turns an inert Au surface into a multi-functional one. As a result, the coated Au is sensitive to the pH due to the presence of amine groups. Furthermore, the AβCyD-based coating can yield a partial or total screening of Au electrode towards electro-active species bearing negative (*viz.* ferricyanide) and positive charges (*viz.* dopamine), respectively. Adsorbed AβCyD vesicles mediate both trapping and release of DA and L-DOPA by using its intrinsic host-guest property. The proper control of the electrical bias allows a gradual drug release not only in a standard electrochemical equipment, but also in an electronic device used as an electronic drug dispenser. Such result opens the way towards bio-electronic applications, because the next generation of hi-tech platforms must be multi-functional in order to manage high-challenging tasks. Among the different functionalities, the release of drug or chemicals is one of the most demanded.

Acknowledgements

This work was supported by the EU-project I-ONE NMP4-SL-2012-280772, and EuroBioSAS-OP-009 (ICS project).

Notes and references

1 Ariga, K.; Ji, Q.; Hill, J. P.; Bando, Y.; Aono, M. Forming Nanomaterials as Layered Functional Structures toward Materials Nanoarchitectonics *NPG Asia Mater.* **2012**, *4*, 1–11.
2 Ariga, K.; Yamauchi, Y.; Rydzek, G.; Ji, Q.; Yonamine, Y.; Wu, K. C.-W.; Hill, J. P. Layer-by-Layer Nanoarchitectonics: Invention, Innovation and Evolution *Chem. Lett.* **2014**, *43*, 36–68.
3 Szejtli, J. Introduction and General Review of Cyclodextrin Chemistry *Chem. Rev.* **1998**, *98*, 1743–1753.
4 Bilensoy, E.; Hincal, A. A. Recent Advances and Future Directions in Amphiphilic Cyclodextrin Nanoparticles *Expert Opin. Drug Deliv.* **2009**, *6*, 1161–1173.
5 Ravoo, B. J.; Darcy, R. Cyclodextrin Bilayer Vesicles *Angew. Chemie Int. Ed.* **2000**, *39*, 4324–4326.
6 Mazzaglia, A.; Valerio, A.; Micali, N.; Villari, V.; Giuffre, M.; Quaglia, F.; Castriciano, A.; Monsu, L.; Siracusano, G.; Sciortino, M. T. Effective Cell Uptake of Nanoassemblies of a Fluorescent Amphiphilic Cyclodextrinand an Anionic Porphyrin *Chem. Commun.* **2011**, 9140–9142.
7 McMahon, A.; O'Neill, M. J.; Gomez, E.; Donohue, R.; Forde, D.; Darcy, R.; O'Driscoll, C. M. Targeted Gene Delivery to Hepatocytes with Galactosylated Amphiphilic Cyclodextrins *J. Pharm. Pharmacol.* **2012**, *64*, 1063–1073.
8 Scala, A.; Cordaro, M.; Mazzaglia, A.; Risitano, F.; Venuti, A.; Sciortino, M. T.; Grassi, G. Synthesis and Anti HSV-1 Evaluation of Novel Indole-3,4-diones *Medchemcomm* **2011**, *2*, 172.
9 Quaglia, F.; Ostacolo, L.; Mazzaglia, A.; Villari, V.; Zaccaria, D.; Sciortino, M. T. The Intracellular effects of Non-IonicAmphiphilic Cyclodextrin Nanoparticles in the Delivery of Anticancer Drugs *Biomaterials* **2009**, *30*, 374–3782.
10 Conte, C.; Scala, A.; Siracusano, G.; Leone, N.; Patanè, S.; Ungaro, F.; Miro, A.; Sciortino, M. T.; Quaglia, F.; Mazzaglia, A. Nanoassembly of an Amphiphilic Cyclodextrin and Zn(II)-phthalocyanine with the Potential for Photodynamic Therapy of Cancer *RSC Adv.* **2014**, *4*, 43903–43911.
11 Mazzaglia, A.; Bondì, M. L.; Scala, A.; Zito, F.; Barbieri, G.; Crea, F.; Vianelli, G.; Mineo, P.; Fiore, T.; Pellerito, C.; Pellerito, L.; Costa, M. A. Supramolecular Assemblies Based on Complexes of Nonionic Amphiphilic Cyclodextrins and a Meso-Tetra(4-sulfonatophenyl)porphyrine Tributyltin(IV) Derivative: Potential Nanotherapeutics against Melanoma *Biomacromolecules* **2013**, *14*, 3820–3829.
12 Kandoth, N.; Vittorino, E.; Sciortino, M. T.; Parisi, T.; Colao, I.; Mazzaglia, A.; Sortino, S. A Cyclodextrin-Based Nanoassembly on Bimodal Photodynamic Action *Chemistry* **2012**, *18*, 1684–1690.
13 Villari, V.; Mazzaglia, A.; Darcy, R.; O'Driscoll, C. M.; Micali, N. Nanostructures of Cationic Amphiphilic

CyclodextrinComplexes with DNA *Biomacromolecules* **2013**, *14*, 811–817.
14 Trapani, M.; Romeo, A.; Parisi, T.; Sciortino, M. T.; Patanè, S.; Villari, V.; Mazzaglia, A. Supramolecular Hybrid Assemblies Based on Gold Nanoparticles, Amphiphilic Cyclodextrin and Porphyrins with Combined Phototherapeutic Action *RSC Adv.* **2013**, *3*, 5607–5614.
15 Mazzaglia, A.; Monsu, L.; Mezzi, A.; Kaciulis, S.; Caro, T. De; Ingo, G. M.; Padeletti, G. Supramolecular Colloidal Systems of Gold Nanoparticles/AmphiphilicCyclodextrin: a FEM-SEM and XPS Investigation of Nanostructures Assembled onto Solid Surface *J. Phys. Chem. C* **2009**, *113*, 12772–12777.
16 Valli, L.; Giancane, G.; Mazzaglia, A.; Scolaro, L. M.; Conoci, S.; Sortino, S. Photoresponsive Multilayer Films by Assembling Cationic Amphiphilic Cyclodextrins and Anionic Porphyrins at the Air/Water Interface *J. Mater. Chem.* **2007**, *17*, 1660–1663.
17 Kergoat, L.; Herlogsson, L.; Braga, D.; Piro, B.; Pham, M.-C.; Crispin, X.; Berggren, M.; Horowitz, G. A Water-Gated Organic Field-Effect Transistor *Adv. Mater.* **2010**, *22*, 2565–2569.
18 Kergoat, L.; Piro, B.; Berggren, M.; Horowitz, G.; Pham, M.-C. Advances in Organic Transistor-Based Biosensors: from Organic Electrochemical Transistors to Electrolyte-Gated Organic Field-Effect Transistors *Anal. Bioanal. Chem.* **2012**, *402*, 1813–1826.
19 Campana, A.; Cramer, T.; Simon, D. T.; Berggren, M.; Biscarini, F. Electrcardiographic Recording with Conformable Organic Electrochemical Transistor Fabricated on Resorbable Scaffold *Adv. Mater.* **2014**, *26*, 3874–3878.
20 Khodagholy, D.; Doublet, T.; Quilichini, P.; Gurfinkel, M.; Leleux, P.; Ghestem, A.; Ismailova, E.; Hervé, T.; Sanaur, S.; Bernard, C.; Malliaras, G. G. In Vivo Recordings of Brain Activity using Organic Transistors *Nat. Commun.* **2013**, *4*, 1575.
21 Kim, D.-H.; Lu, N.; Ghaffari, R.; Kim, Y.-S.; Lee, S. P.; Xu, L.; Wu, J.; Kim, R.-H.; Song, J.; Liu, Z.; Viventi, J.; de Graff, B.; Elolampi, B.; Mansour, M.; Slepian, M. J.; Hwang, S.; Moss, J. D.; Won, S.-M.; Huang, Y.; Litt, B.; Rogers, J. A. Materials for Multifunctional Balloon with Capabilites in Cardiac Electrophysiological Mapping and Ablation Therapy *Nat. Mater.* **2011**, *10*, 316–323.
22 Viventi, J.; Kim, D.-H.; Moss, J. D.; Kim, Y.-S.; Blanco, J. a; Annetta, N.; Hicks, A.; Xiao, J.; Huang, Y.; Callans, D. J.; Rogers, J. a; Litt, B. A Conformal, Bio-Interfaced Class of Silicon Electronics for Mapping Cardiac Electrophysiology *Sci. Transl. Med.* **2010**, *2*, 24ra22.
23 Viventi, J.; Kim, D.-H.; Vigeland, L.; Frechette, E. S.; Blanco, J. a; Kim, Y.-S.; Avrin, A. E.; Tiruvadi, V. R.; Hwang, S.-W.; Vanleer, A. C.; Wulsin, D. F.; Davis, K.; Gelber, C. E.; Palmer, L.; Van der Spiegel, J.; Wu, J.; Xiao, J.; Huang, Y.; Contreras, D.; Rogers, J. A; Litt, B. Flexible, Foldable, Actively Multiplexed , High-Density Electrode Array for Mapping Brain Activity In-Vivo *Nat. Neurosci.* **2011**, *14*, 1599–1605.
24 Son, D.; Lee, J.; Qiao, S.; Ghaffari, R.; Kim, J.; Lee, J. E.; Song, C.; Kim, S. J.; Lee, D. J.; Jun, S. W.; Yang, S.; Park, M.; Shin, J.; Do, K.; Lee, M.; Kang, K.; Hwang, C. S.; Lu, N.; Hyeon, T.; Kim, D.-H. Multifunctional Wearable Devices for Diagnosis and Therapy of Movement Disorders *Nat. Nanotechnol.* **2014**, *9*, 397–404.
25 Minev, I. R.; Musienko, P.; Hirsch, A.; Barraud, Q.; Wenger, N.; Moraud, E. M.; Gandar, J.; Capogrosso, M.; Milekovic, T.; Asboth, L.; Torres, R. F.; Vachicouras, N.; Liu, Q.; Pavlova, N.; Duis, S.; Larmagnac, A.; Vörös, J.; Micera, S.; Suo, Z.; Courtine, G.; Lacour, S. Electronic Dura Mater for Long-Term Multimodal Neural Interfaces *Science* **2015**, *347*, 159–163.
26 Ferancová, A.; Labuda, J. Cyclodextrins as electrode modifiers *Fresenius J. Anal. Chem.* **2001**, 370, 1-10.
27 Cristiano, A.; Lim., C.W.; Rozkiewicz., D.I.; Reinhoudt, D.N.; Ravoo, B.J. Solid-supported monolayersand bilayersof amphiphilic β-cyclodextrins *Langmuir* **2007**, 8944-8949.
28 Silvestre, J.P.; Pouline, S.; Kabashin, A.V.; Sacher, E.; Meunier, M.; Luong, J.H.T. Surface Chemistry of Gold Nanoparticles Produced by Laser Ablation in Aqueous Media *J. Phys. Chem. B* **2004**, 108, 16864-16869.
29 Reviakine, I.; Brisson, A.; Formation of supported phospholipid bylayer from unilamellar vesicles investigated by atomic force microscopy *Langmuir*, **2000**, 16, 1806-1815.
30 Sackmann, A. Supported membrane: Scientific and practical applications *Science*, **1996**, 71, 43-48.
31 Krim, J.; Palasantzas, G. Experimental Observations of Self-Affine Scaling and Kinetic Roughening at Sub-Micron Lengthscales *Int. J. Mod. Phys. B* **1995**, *09*, 599–632.
32 Albonetti, C.; Casalini, S.; Borgatti, F.; Floreano, L.; Biscarini, F. Morphological and Mechanical Properties of Alkanethiol Self-Assembled Monolayers Investigated Atomic Force Microscopy *Chem. Commun. (Camb).* **2011**, *47*, 8823–8825.
33 Donohue, R.; Mazzaglia, A.; Ravoo, B. J.; Darcy, R. Cationic β-Cyclodextrin Bilayer Vesicles *Chem. Commun. (Camb).* **2002**, *7*, 2864–2865.
34 Bard, A. J.; Faulkner, L. R. *Electrochemical Methods Fundamentals and Applications*; 2001.
35 Park, S.-M.; Yoo, J.-S. Electrochemical Impedance Spectroscopy for Better Electrochemical Measurements *Anal. Chem.* **2003**, *75*, 455–461.
36 Mark, L. W.; Smith, D. A. Complex Chemical Force TitrationBehavior of Amine-Terminated Self-Assembled Monolayers *Langmuir* **2001**, *17*, 1126–1131.
37 Dryhurst, G.; Kadish, M. K.; Scheller, F.; Renneberg, R. *Biological Electrochemistry volume 1*; Academic Press, 1982.
38 Sanchez-Rivera, A. E.; Corona-Avendaño, S.; Alarcón-Ángeles, G.; Rojas-Hernández, A. .; Ramírez-Silva, M. T.; Romero-Romo, M. A. Spectrophotometric Study on the Stability of Dopamine and the Determination of its Acidity Constants *Spectrochim. Acta Part A* **2003**, *59*, 3193–3203.
39 Abbaspour, A.; Noori, A. A Cyclodextrin Host-Guest Recognition Approach to an Electrochemical Sensor for Simultaneous Quantification of Serotonin and Dopamine *Biosens. Bioelectron.* **2011**, *26*, 4674–4680.
40 Palomar-Pardavé, M.; Corona-Avendaño, S.; Romero-Romo, M.; Alarcón-Angeles, G.; Merkoçi, a.; Ramírez-Silva, M. T. Supramolecular Interaction of Dopamine with β-Cyclodextrin: An Experimental and Theoretical Electrochemical Study *J. Electroanal. Chem.* **2014**, *717-718*, 103–109.
41 Shityakov, S.; Broscheit, J.; Förster, C. α-Cyclodextrin Dimer Complexes of Dopamine and Levodopa Derivatives to Assess Drug Delivery to the Central Nervous System: ADME and Molecular Docking Studies *Int. J. Nanomedicine* **2012**, *7*, 3211–3219.
42 Tan, L.; Zhou, K.-G.; Zhang, Y.-H.; Wang, H.-X.; Wang, X.-D.; Guo, Y.-F.; Zhang, H.-L. Nanomolar Detection of Dopamine in the Presence of Ascorbic Acid at β-Cyclodextrin/Graphene Nanocomposite Platform *Electrochem. commun.* **2010**, *12*, 557–560.
43 Yang, J.-H.; Kim, H. T.; Kim, H. A Cyclodextrin-Based Approach for Selective Detection of Catecholamine Hormone Mixtures *Micro Nano Syst. Lett.* **2014**, *2*, 1–10.
44 Zachek, M. K.; Hermans, A.; Wightman, R. M.; McCarty, G. S. Electrochemical Dopamine Detection: Comparing Gold and Carbon Fiber Microelectrodes Using Background Subtracted Fast Scan Cyclic Voltammetry *J. Electroanal. Chem.* **2008**, *614*, 113–120.
45 Zerbino, J. O.; Sustersic, M. G. Ellipsometric and Electrochemical Study of Dopamine Adsorbed on Gold Electrodes *Langmuir* **2000**, *16*, 7477–7481.

46 Kergoat, L.; Piro, B.; Berggren, M.; Pham, M.-C.; Yassar, A.; Horowitz, G. DNA Detectionwith Water-Gated Organic Field-Effect Transistor *Org. Electron.* **2012**, *13*, 1–6.
47 Buth, F.; Donner, A.; Sachsenhauser, M.; Stutzmann, M.; Garrido, J. A. Biofunctional Electrolyte-Gated Organic Field-Effect Transistors *Adv. Mater.* **2012**, *24*, 4511–4517.
48 Magliulo, M.; Mallardi, A.; Mulla, M. Y.; Cotrone, S.; Pistillo, B. R.; Favia, P.; Vikholm-Lundin, I.; Palazzo, G.; Torsi, L. Electrolyte-Gated Organic Field-Effect Transistor Sensors Based on Supported Biotinylated Phospholipid Bilayer *Adv. Mater.* **2012**, 1–5.
49 Casalini, S.; Leonardi, F.; Cramer, T.; Biscarini, F. Organic Field-Effect Transistorfor Label-Free Dopamine Sensing *Org. Electron.* **2013**, *14*, 156–163.
50 Casalini, S.; Dumitru, A. C.; Leonardi, F.; Bortolotti, C. A.; Herruzo, E. T.; Campana, A.; Oliveira, R. F. De; Cramer, T.; Garcia, R.; Biscarini, F. Multiscale Sensing of Antibody-Antigen Interactions by Organic Transistors and Single-Molecule Force Spectroscopy M. *ACS Nano* **2015**, *9*, 5051–5062.
51 Kergoat, L.; Herlogsson, L.; Braga, D.; Piro, B.; Pham, M.-C.; Crispin, X.; Berggren, M.; Horowitz, G. *Adv. Mater.* **2010**, *22*, 2565–2569.
52 Cramer, T.; Kyndiah, A.; Murgia, M.; Leonardi, F.; Casalini, S.; Biscarini, F. Double Layer Capacitance Measured by Organic Field-Effect Transistor Operated in Water *Appl. Phys. Lett.* **2012**, *100*, 143302.
53 Guo, J.; Koch, N.; Schwartz, J.; Bernaseck, SL. Direct measurement of surface complex surface loading and surface dipole and their effect behavior *J. Phys. Chem. B* **2005**, 109, 3966-3970.
54 Leonardi, F; Casalini, S.; Albonetti, C.; Kovtun, A.; Liscio, A.; Biscarini, F. Charge-injection organic gauges to detect dopamine down to the nanomolar scale *IEEE Trans. Electron. Dev.* in press doi: 10.1109/TED.2015.2491650.
55 Casalini, S.; Shehu, A.; Destri, S.; Porzio, W.; Pasini, M. C.; Vignali, F.; Borgatti, F.; Albonetti, C.; Leonardi, F.; Biscarini, F. Organic Field-Effect Transistors as New Paradigm for Large-Area Molecular Junctions *Org. Electron.* **2012**, *13*, 789–795.
56 Baikie, I.D.; Mackenzie, S.; Estrup, P.J.Z.; Meyer, J.A. Noise and Kelvin Method *Rev. Sci. Instrum.* **1991**, 62, 1326-1333.
57 Casalini, S.; Shehu, A.; Leonardi, F.; Albonetti, C.; Borgatti, F.; Biscarini, F. Hydrophylic Self-Assembly Monolayers for Pentacene-Based Thin-Film Transistors *Org. Electron.* **2013**, *14*, 1891–1897.